Accepted Manuscript

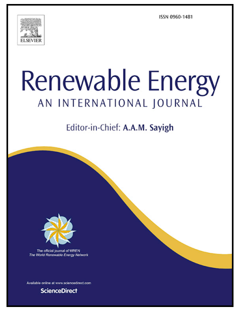

Potential uses of a prototype linear Fresnel concentration system

Pablo Dellicompagni, Judith Franco

PII: S0960-1481(18)31189-3

DOI: 10.1016/j.renene.2018.10.005

Reference: RENE 10654

To appear in: *Renewable Energy*

Received Date: 19 February 2018

Revised Date: 24 July 2018

Accepted Date: 1 October 2018

Please cite this article as: Dellicompagni P, Franco J, Potential uses of a prototype linear Fresnel concentration system, *Renewable Energy* (2018), doi: https://doi.org/10.1016/j.renene.2018.10.005.

POTENTIAL USES OF A PROTOTYPE LINEAR FRESNEL CONCENTRATION SYSTEM

1. Abstract

This study analyzes the energy potential of a linear Fresnel solar (LFS) system based on a case study of the equipment mounted in the city of San Carlos, Salta province, Argentina. The average thermal power and thermal losses from the absorber and field pipes to the environment were calculated by hour, taking into account the hourly direct normal irradiance (DNI) obtained by Liu-Jordan method, based on global horizontal irradiation (GHI) measurements. This paper shows the amount of thermal energy that the LFS under study is able to generate for processes such as hard water desalination, electric power generation, and drying of vegetables. The results of the calculations show that the linear Fresnel system is capable of producing steam with thermal energy in the range of 460 - 1200 MJ_{th}, which means an annual production of 243 GJ_{th}. As for the power block, it is possible to obtain an annual generation of 1.5 GWh_e, depending on operating conditions of the steam engine (288 rpm regime at 6 bar). The production of desalinated water reaches the range of 98 - 112 m^3, depending on whether the steam is previously used for power electric generation or not.

Keywords: Linear Fresnel; thermal power; desalination; power generation.

2. Introduction

Linear solar concentration is a viable and cost-effective technology with a promising future. If the working fluid is water, steam can be directly generated in the absorber without costly intermediate heat exchangers. There are two types commonly developed by industry: parabolic trough (PTC) and Linear Fresnel (LFC). Both have been extensively studied and characterized, with special interest on large-scale systems for on-grid electricity generation (Hachicha et al., 2018; Elsafi, 2015; Serrano – Aguilera et al., 2017; Qui Yu et al., 2017; Cagnoli et al., 2018; Tsekouras et al., 2018). On the other hand, studies on small-scale concentrating systems – which provide heat outputs in the range of 150 – 300 °C are scarce. These systems have promissory applications in combined heat and power generation (Heimsath et al., 2010) water desalination (Borunda et al., 2016), heating/cooling of buildings (Zhou et al., 2017; Bermejo et al., 2010), advanced absorption air cooling using Solar-GAX cycle (Velázquez et al., 2010), domestic water heating (Mokhtar et al., 2016; Sultana et al., 2010) steam generation for mining, and also in textile, paper and chemical industries, timber, food, and agriculture (Barbón et al., 2018; Zhu and Chen, 2018). The great potential of this technology was highlighted by Rawlins and Ashcroft (2013) who predict a growth of small-scale systems for industrial processes of about 2.5 (globally) and 4.6 (in Latin America and Africa), from now to 2050. The large variety of possible applications of small systems is promissory, but further research is needed in order to characterize their thermodynamic and energy behavior.

The utilization of energy of all thermodynamic cycles relies heavily on the efficiency of their parts. Generally, the purpose is to optimize the components of a given thermo-energetic installation so that, overall, the utilization of energy takes place in optimal conditions. It is also possible to optimize the *thermal performance* of a system, like a solar plant, by calibrating the working temperature and pressure (Lin et al., 2013). One of the most important design parameters for a compact solar plant (CSP) is *design irradiance*, which is the direct normal irradiance (DNI) at which the plant produces the nominal electric power. Due to the daily and seasonal variation in radiation, determining appropriate design irradiance is extremely important; low design irradiance results in excessive unutilized energy, and high design irradiance results in low capacity factor of the plant (Desai et al., 2014). The net energy capable of being transformed into useful or usable energy is influenced by thermodynamic, mechanical, or strategic parameters, according to the use of the available thermal energy.

This study analyzes the energy potential of a linear Fresnel solar (LFS) system for different strategies for uses of thermal energy contained in the steam based on a case study of the equipment mounted in the city of San Carlos, Salta province, Argentina (Saravia et al., 2014; Hongn et al., 2015). There is no other similar technology in Argentina neither in South America. Furthermore, this equipment was built with 100 percent of local materials whose are easy to obtain in the region. This represents an advantage to decide which technology to use for solar concentration and thermal generation.

First, this work presents the solar gain in the absorption system and then the successive energetic transformations within a Rankine type closed system for four variants: i) direct steam feed to a condenser; ii) power generation; iii) hard water desalination and iv) both process together, power generation and desalination. Each stage is studied from an analytical, theoretical, and experimental perspective, on the basis of *in situ* measurements and computational simulations (Hongn, 2017; Hongn et al., 2015; Dellicompagni et al., 2015 – 2016 – 2018). The energy flow and the energy losses are analyzed from the solar gain in the absorber to the condenser inlet. The aim of this analysis is to determine the energy available for different applications, such as fruit and vegetable kilns, greenhouses, vegetable oil extraction, water desalination, etc.

3. The thermodynamic cycle

The LFS system installed in the city of San Carlos (Saravia et al., 2014) uses the conventional Rankine cycle with water steam as the heat-transfer fluid (HTF). This is the most widely used type of cycle in solar concentration plants (Desai et al., 2014), though other configurations also exist, such as the Kalina cycle, used in solar plants as background cycle (Mittelman and Epstein, 2010).

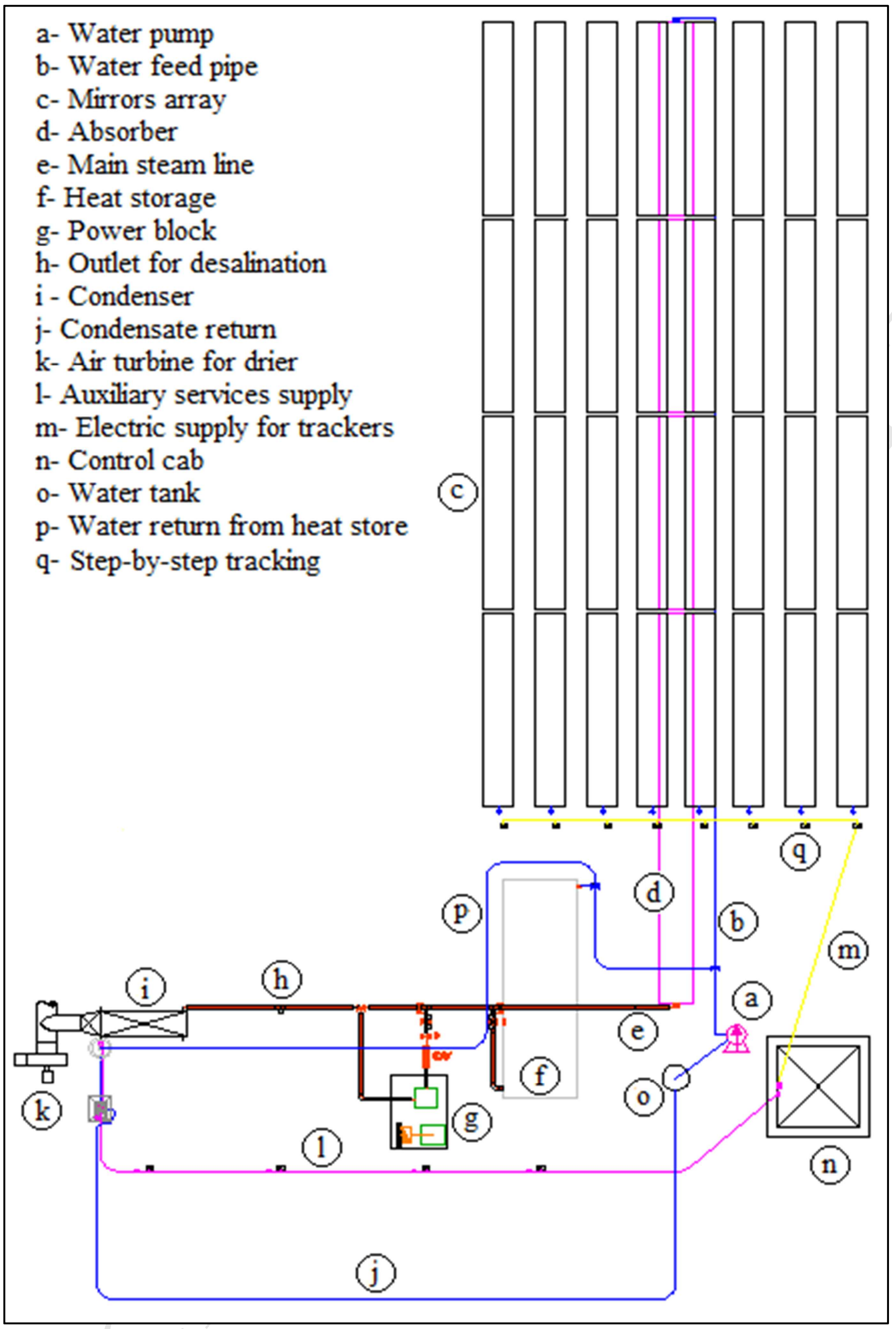

Figure 1. Scheme of the installation and circulation of fluids.

Figure 1 shows the current configuration of the Fresnel pilot plant of San Carlos. It has a positive displacement pump (a), which pressurizes the water coming from the tank (o) to the inlet of the absorber (d). Then heat gain and evaporation of the HTF take place. When is possible, the water steam is used for thermal storage (f), power generation (g), or desalination (h). It means that the steam can circulate to several consumers.

The residual steam is used to preheat the air from the environment that will be injected into the dryer chamber by means of a turbine (k). This thermal exchange takes place in the condenser (i). After that, the condensate is pumped into the tank through the return pipe (j). In addition, the equipment has a control cabinet (n) for power supply to auxiliary circuits (l) and step-by-step motors (q) for solar tracking. This LFS combines with another passive solar collection system (Condorí et al., 2009), which makes the drying process more versatile. This is a passive one that uses solar gain to heat the environmental air. Both air, the heated by steam/condenser as well as passive system, are mixed in the main duct before the fan-turbine. This passive solar collector is used when the Fresnel System is no operating.

Table 1 presents some parameters of the LFS under study (Hongn, 2017; Flores Larsen and Hongn, 2014).

Table 1. Specifications of the absorber and reflector field.

Parameters	Dimensions
Number of tubes	5
Total length of the absorber	30 m
Inner diameter of the head pipe, d_i	26.6 mm
Outer diameter of the head pipe, d_o	33.4 mm
Area of absorber pipes, A_{abs}	3.05 m^2
Mirror level height of the absorber, H	6.96 m
Thermal conductivity of the collector pipes	64 W m^{-1} k^{-1}
Collection area, Ac	172 m2
Area per row of mirrors, A_i	21.5 m2

4. Incident thermal power and thermal losses

The city of San Carlos is located in a favorable area for harnessing solar energy (Lat. -25.88; Long. -65.33). Grossi Gallegos et al. (2009) studied the solar resource in this city through the Solarimetric network (G. Gallegos & Righini, 2007; Raichijk et al., 2008), by calculating the average global daily irradiation (kWh/m^2). They also analyzed the probability of occurrence of consecutive cloudy days. The study concluded that global horizontal irradiation (GHI) reaches maximum values of 6.5 kWh/m^2 (23.4 MJ/m^2) in November and December, and minimum values of approximately 3.5 kWh/m^2 (12.6 MJ/m^2) in June. Measurements carried out in the place where the LFS is located indicated that the daily average global horizontal irradiation (DAGHI) reaches 28.7 MJ/m^2 in summer (Figure 2).

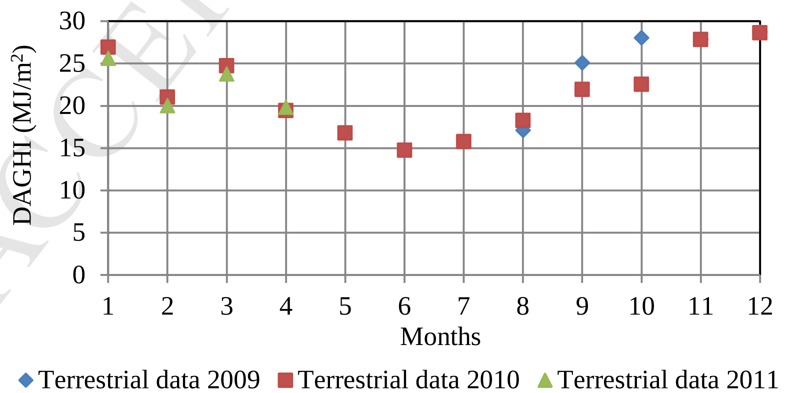

Figure 2. Global horizontal irradiation terrestrial data measured in San Carlos.

Unfortunately, there are no measurements of direct normal irradiation (DNI) for San Carlos. However, it is possible to obtain DNI and diffuse components of solar irradiation from estimation models such as the hybrid Yang model (Yang et al., 2001) and Liu-Jordan (Duffie–Beckman, 2005). Yang model calculates direct and diffuse components taking into account terrestrial measurements of temperature, humidity, and turbidity. If turbidity is unavailable, the Ångström's technique is commonly used (Ångström, 1961). Liu-Jordan model considers the daily average of GHI measured in the location.

To determine the incident thermal power $\dot{Q}i$, for the case without blocking or shading, equation 1 could be applied (Altamirano, 2014).

$$\dot{Q}i = \sum_1^8 DNI_i \cdot A_i \quad (1)$$

However, this equation does not quantify the real gain, because certain factors further reduce the amount of irradiance that reaches the absorber. The average hourly thermal power (W) absorbed by the HTF is calculated as follows (Hongn, 2017 - 2018):

$$\dot{Q}_a = \dot{Q}_i - \Delta\dot{Q}_{ia} \quad (2)$$

where:

$$\dot{Q}_i = DNI \cdot F_e \cdot (\tau \cdot \alpha) \cdot \sum_{i=1}^8 A_i \cdot \rho_i \cdot \cos\theta_i \cdot f_i \cdot F_i \quad (3)$$

$$\Delta\dot{Q}_{ia} = U_L \cdot A_{abs} \cdot \left(T_{pipe} - T_{ambient}\right) \quad (4)$$

where:

$$U_L = 0.357 \cdot (T_{pipe} - T_{ambient})^{0.5184} W/m^2K \quad (5)$$

Equation 5 for global heat loss was determined by Flores Larsen et al. (2012) in laboratory tests. These measurements were performed on a Fresnel model of absorber at a real geometrical scale, but with a length of 1.4 m and an insulating cover. T_{pipe} is the average temperature of the absorber pipes and $T_{ambient}$ is the ambient temperature of the place where the tests were carried out. Equation 5 gives global heat loss values between 3 and 6 W/m^2K, in line with Singh et al. (2010a, 2010b), Khan (1999), and Negi et al. (1989), who determined that the power curve may be attributed to the dominance of radiation losses, which increases significantly with temperature. The geometry and materials of the absorber reported by Flores Larsen (2012) are more similar to those reported by Singh et al (2010a, 2010b). Other studies of absorbers with non-evacuated tubes gave values of 2.0 W/mK (Häberle et al., 2002), 1.25 W/mK (Feuermann et al., 1991), and 1.0 W/mK (Facão et al., 2011). It is important to note that there are significant differences between the mentioned absorbers, such as the number of tubes, the geometry, the infrared emittance due to the selective paintings, the use of CPC cavities, etc., and these differences explain the variations in the values of the overall heat loss coefficients.

The coefficient f_i is the illuminated fraction of the absorber (end effect). In addition, the cosine effect ($\cos\theta_i$) (Morin et al., 2012), the cleanliness factor (F_e), the reflectivity of reflectors (ρ_i), the intercept factor of receiver (F_i), the transmissivity of the receiver cover (τ), and the absorptivity of the absorber tubes (α) contribute to energy losses. All the values of these factors were calculated by Hongn (2017) in hourly terms for all characteristic days of the year.

Several authors (Carvalho et al., 2007; Mertins, 2008; Wagner and Zhu, 2012; Baniasad Askari and Ameri, 2018) consider the transversal incidence angle modifier (IAM) K_t (for varying angle θ_{it}) and the longitudinal IAM K_l (for varying angle θ_{il}), obtained by simulation using radiation tracking programs. However, there is no IAM calculation for the current case study yet, and this is the reason why IAM factors were not considered in equation 3.

The hourly energy calculation is performed for the characteristic Julian day of every month, taking into account the DNI values obtained by Liu-Jordan method based on daily average GHI (Figure 3). Operating time is assumed to be from 10 a.m. to 5 p.m. because a DNI of at least 400 W/m^2 is considered necessary to generate steam with the equipment in a thermal regime.

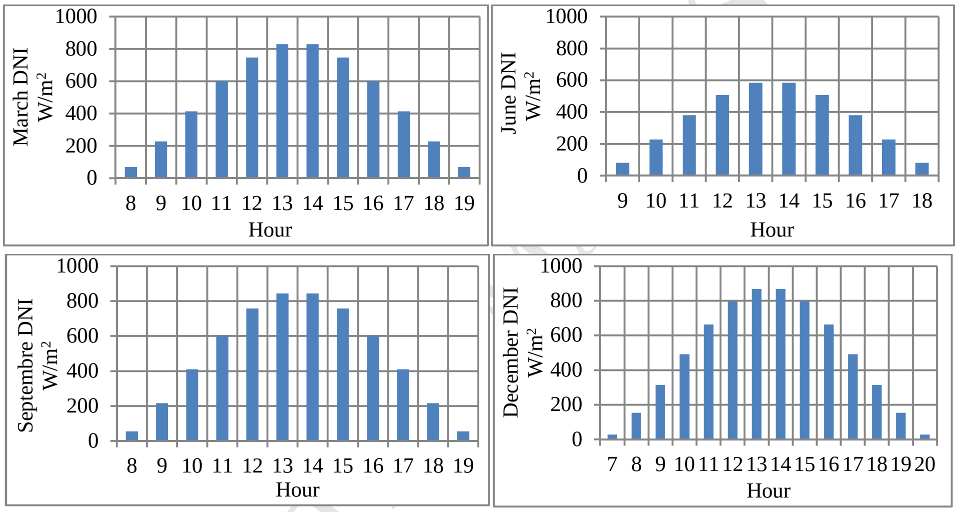

Figure 3. Hourly DNI values for the most representative months.

Thermal losses from the pipes are also considered for the energy calculation. The main steam-line of the LFS has insulated and non-insulated sections, and their respective thermal losses toward the environment are given by equations 6 and 7 (Duffie–Beckman, 2005).

$$\Delta\dot{Q}_{l-i} = \frac{2\pi L\,(T_f - T_e)}{\left[\frac{4}{d_i h_{conv}} + \frac{1}{k_w \ln\left(\frac{d_o}{d_i}\right)} + \frac{1}{k_{ais} \ln\left(\frac{D_i}{d_o}\right)} + \frac{1}{k_{PVC} \ln\left(\frac{D_o}{D_i}\right)}\right]} \tag{6}$$

$$\Delta\dot{Q}_{l-n} = \frac{2\pi L\,(T_f - T_e)}{\left[\frac{4}{d_i h_{conv}} + \frac{1}{k_w \ln\left(\frac{d_o}{d_i}\right)} + \frac{1}{d_o (h_a + h_r)}\right]} \tag{7}$$

Where k_w, k_{ais} and k_{PVC} are the thermal conductivity coefficients of the different materials that compose the steam line (Bergman, 2011), which are galvanized steel, glass wool, and PVC®, respectively; d_i and d_o are the inner and outer diameters of the galvanized steel pipe that carries the HTF, while D_i and D_o are the inner and outer diameters of the PVC® cover, T_f and T_e are the steam and environment temperatures, respectively; L is the length of the insulated pipe or non-insulated section; h_{conv} is the convection coefficient for the steam circulating within the galvanized-steel pipe; h_a is the convection coefficient of the external air and h_r is the coefficient of radiation to the environment and its value is determined by equation 8 (Duffie–Beckman, 2005) where T_o is the temperature of the external surface of the non-insulated section, calculated through successive iteration.

$$h_r = \varepsilon \cdot \sigma \cdot ({T^2}_o + {T^2}_e) \cdot (T_o + T_e) \tag{8}$$

In order to simplify the calculation, outer diameter of the whole non-insulated sections is assumed as the nominal of the installation (do= 26.9 mm).

Both the steam temperature and the steam fraction drop throughout the installation due to the heat transfer to the outer environment. The thermal leap of steam in each section of the installation is analytically determined by means of the mass and energy balances (equations 9 and 10) (Mc Adams, 1954) for a model such as the one shown in Figure 4, where the variables reach a stationary state.

$$\rho_{1(\theta_1,\,x_1)} = \rho_{l(\theta_0+\delta\theta)} + \left(\rho_{g(\theta_0+\delta\theta)} - \rho_{l(\theta_0+\delta\theta)}\right)(x_0 + \delta x) \tag{9}$$

$$f_{l0}\left(h_{0(\theta_0,\,x_0)} - h_{1(\theta_1,\,x_1)}\right) - \dot{Q}_l = 0 \tag{10}$$

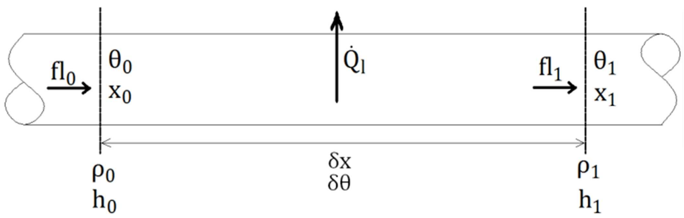

Figure 4. Steam pipe model for variables in stationary state.

Where:

- fl is the steam flux in kg/s.
- x is the steam fraction.
- θ is the steam temperature, in C.
- ρ is the steam/water mixture density, in kg/m^3.
- h is the specific enthalpy of the steam/water mixture, in J/kg.
- δx is the variation in steam fraction.
- δθ is the variation in steam temperature.

The sub-indices “0” and “1” correspond to the initial and final state of the variables, respectively.

The expressions for calculating temperature variation ($\delta\theta$) and steam fraction (δx) derive from the equations of mass and energy balance (equations 11 and 12).

$$(\rho_{gl})_{\theta_0}\delta x + \left[\left(\frac{\partial\rho_l}{\partial\theta}\right)_{\theta_0} + \left(\frac{\partial\rho_{gl}}{\partial\theta}\right)_{\theta_0} x_0\right]\delta\theta = 0 \tag{11}$$

$$(-h_{gl})_{\theta_0}\delta x + \left[\left(\frac{\partial h_g}{\partial\theta}\right)_{\theta_0} + \left(\frac{\partial h_{gl}}{\partial\theta}\right)_{\theta_0} x_0\right]\delta\theta = -\dot{Q}_l/fl_0 \tag{12}$$

Heat loss $\dot{Q}_l$ is given by equations 6 and 7, for insulated and non-insulated pipes, resulting in a system of first-order equations, where ρ_l is the water density contained in the steam; $\rho_{gl} = \rho_g - \rho_l$, where ρ_g is the density of the steam phase; $h_{gl} = h_g - h_l$, where h_l is the enthalpy of the liquid phase, and h_g is the enthalpy of the steam phase, with all the state variables and their derivatives particularized for the value of the initial temperature θ_0. Final temperature and final title, respectively, will be equal to:

$$\theta_1 = \theta_0 + \delta\theta \tag{13}$$

$$x_1 = x_0 + \delta x \tag{14}$$

The steam temperature is measured at the beginning of the main line, as shown in Figure 5. A K-type sensor was used and the data was recorded using a twelve-channel DigiSense datalogger. This temperature is taken as the initial value for the calculation of the decrease in steam temperature along the steam line.

Figure 5. K-type sensor for temperature measurement and main steam line.

5. Thermal energy available for processes

The thermal energy calculation is based on the daily average DNI for each hour and equation 2 gives the thermal energy absorbed by the HTF, $\dot{Q}_a$. Then, equations 6 and 7 give thermal losses of field pipes, which have to be subtracted from $\dot{Q}_a$ to obtain the average hourly thermal power available (Baniasad Askari and Ameri, 2018) (equation 15) to feed different processes such as electric power generation, hard water desalination, and vegetable drying. The average thermal energy (in MJ) is calculated for each hour (3600 s) taking into account the average thermal power available in the steam as a constant. A working pressure of 6 bar is considered for all processes.

$$\dot{Q}_j = \dot{Q}_a - \sum_j \Delta\dot{Q}_{l-i} - \sum_j \Delta\dot{Q}_{l-n} \tag{15}$$

The thermal power of the steam, for each hour, is shown in Figure 6. A range of variation from 4 kW_{th} to 49 kW_{th} is observed. Low values are reported at first hours of sun as well as last hours. Maximum thermal power values are situated in a range of 15 kW_{th} and 49 kW_{th} in the solar midday. This range corresponds to that determined by Hongn (2017) through his model developed in Python, obtaining a maximum thermal power of 43.5 kW_{th}.

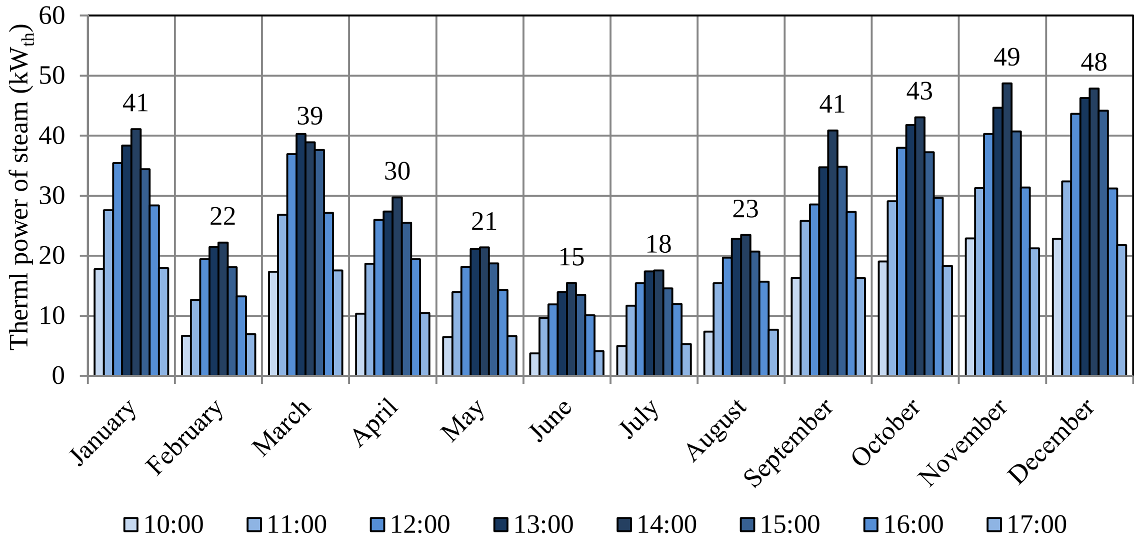

Figure 6. Hourly thermal power of the steam for each characteristic day.

The thermal efficiency of the absorber, for steam production, is defined by equation 16 and its hourly variation, for characteristic days of each month, is shown in Figure 7.

$$\eta_{th} = \frac{\dot{Q}_a}{DNI \sum_{i=1}^{8} A_i} \qquad (16)$$

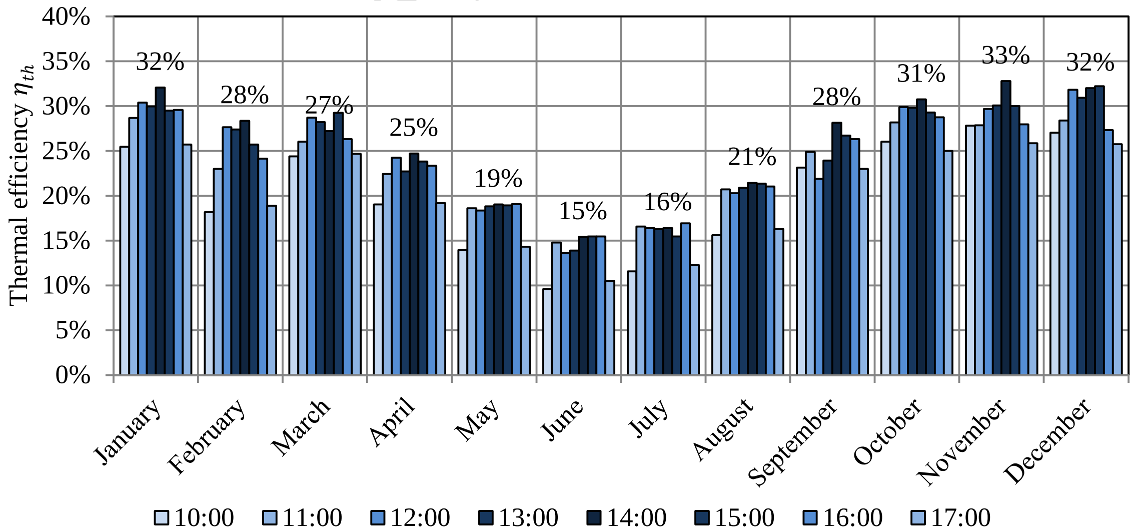

Figure 7. Hourly variation for thermal efficiency of steam generation at the absorber.

The results of thermal power and thermal efficiency obtained in the present study are closely comparable with results of other authors, and even with the results obtained by

Hongn (2017) for the same Fresnel System. The comparison of main parameters is shown in Table 2.

Table 2. Comparison of results for real cases and the actual case study.

Author	Location	Field mirror (m^2)	Thermal Power (kW_{th})	Thermal efficiency (%)	Temperature of steam (ºC)
Lin et al., 2013	Shanghai	14.4	-	37 – 45	90 – 150
Bermejo et al., 2010	Sevilla	352	60 – 180	16 – 24	180
Hongn, 2017	San Carlos	172	43.5	20 – 45	160 – 170
Actual study	San Carlos	172	15 – 49	15 – 33	160 – 180

5.1. *Direct injection of steam in the dryer*

The generated steam is used to pre-heat the air from the environment to introduce it into the drying chamber. Thermal transference takes place by means of the steam-air condenser type. Figure 8 shows the values of thermal energy available in each section of the steam line where the different steam consumers are connected.

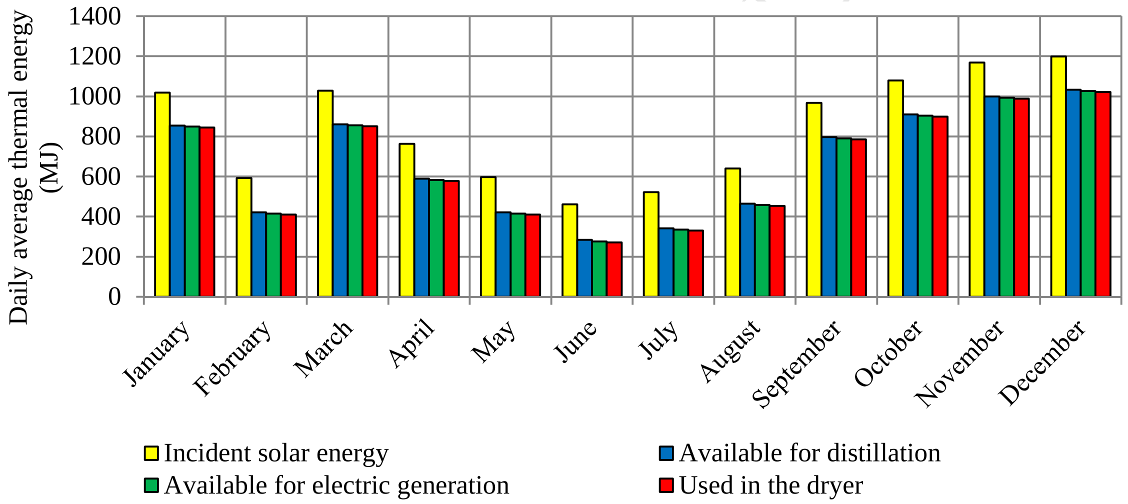

Figure 8. Incident solar thermal energy, energy available for desalination, energy available for power generation, and energy used in the dryer.

As shown in Figure 8, relatively low values are observed in February, due to the climatic conditions of cloudiness and precipitation, typical characteristics of the valleys in the province of Salta. The working temperature is obtained by regulating the pressure with the control valves. Figure 9 shows how the steam temperature decreases due to the thermal losses of the pipes. For months of high temperature, the average relative decrease is -0.61 °C/m, and slightly higher for months of low temperature, -0.67 °C/m. Both curves correspond to the thermal state of the system at 14 p.m.

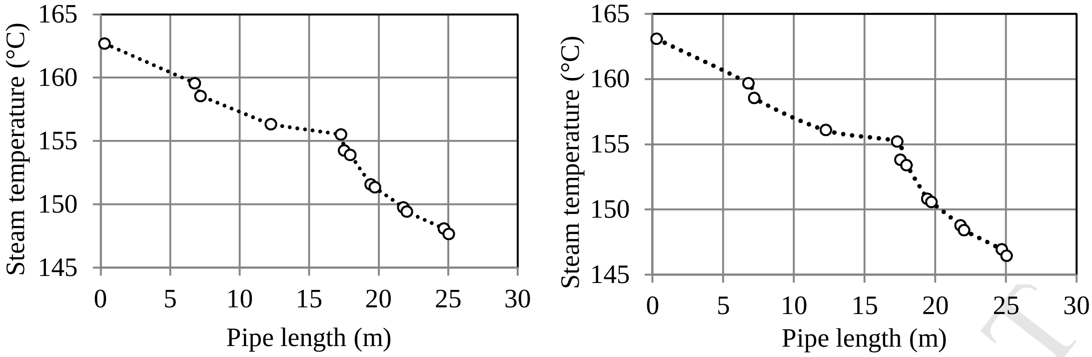

Figure 9. Decrease in the steam temperature throughout the installation, from end of absorber to condenser inlet. Left: January. Right: June.

5.2. *Electric power generation*

Electric power generation occurs before the steam goes into the condenser. Electric power, in kWh_e, is calculated by equation 17. Then, the residual steam is used in the condenser and this steam releases its thermal energy and pre-heats the environment air for the drying process.

$$EE = 3600 \cdot \left(N_u \cdot \eta_{tr} \cdot \eta_{gr}\right)/(3.6\,kWh_e/MJ) \quad (17)$$

$\boldsymbol{\eta_{tr}}$ and $\boldsymbol{\eta_{gr}}$ are the mechanical efficiency of the transmission and electric efficiency of the tree-phase generator, respectively. Effective mechanical power developed by the steam engine (N_u) was determined by experimental measurements with a torque-meter built for this purpose (Figure 10).

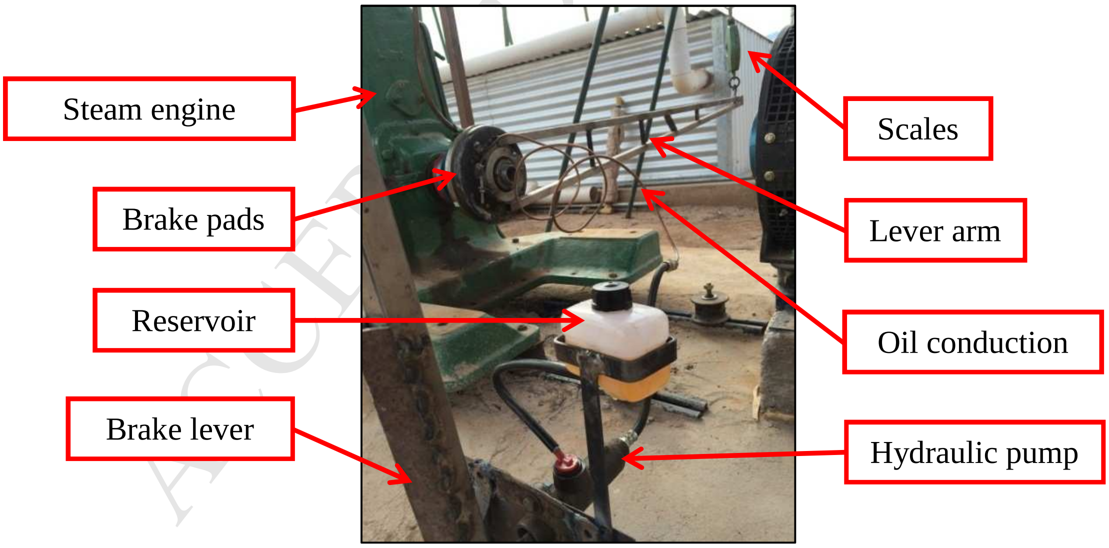

Figure 10. Torque-meter for measurements of effective mechanical power.

Measurements are performed in an indirect way, by manually activating the brake until the revolution regime becomes permanent. At this point, a reading of the brake force is taken on the scales located at the end of the lever. Effective power in Watts is equal to:

$$N_u = 0{,}69869 \cdot F \cdot n \quad (18)$$

Where brake force F is measured in pounds (scales unit) and speed regime in rpm. The effective power of the steam engine is obtained for different working pressures (Figure 11).

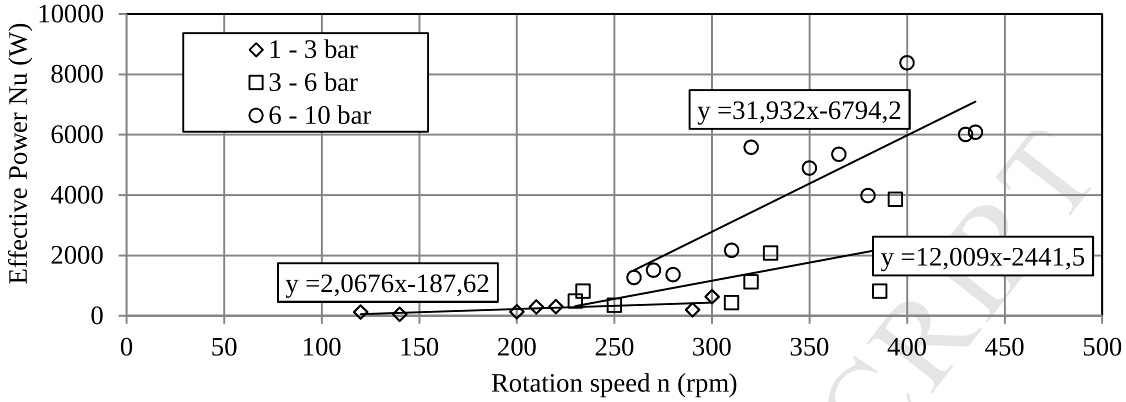

Figure 11. Effective mechanical power developed by the steam engine, as a function of rpm and for different admission pressures. For a regime of 288 rpm and a working pressure of 6 bar, the steam engine generates an effective mechanical power of 2.4 kW.

Figure 12 shows the available thermal energy for desalination and drying processes, when steam is used to generate electrical energy. In relative terms, the mechanical energy developed by the steam engine is small, and this is due to the top mechanical power engine for a speed of 288 rpm. This power increases if the rpm regime increases or if the intake steam pressure increases, as seen in Figure 11.

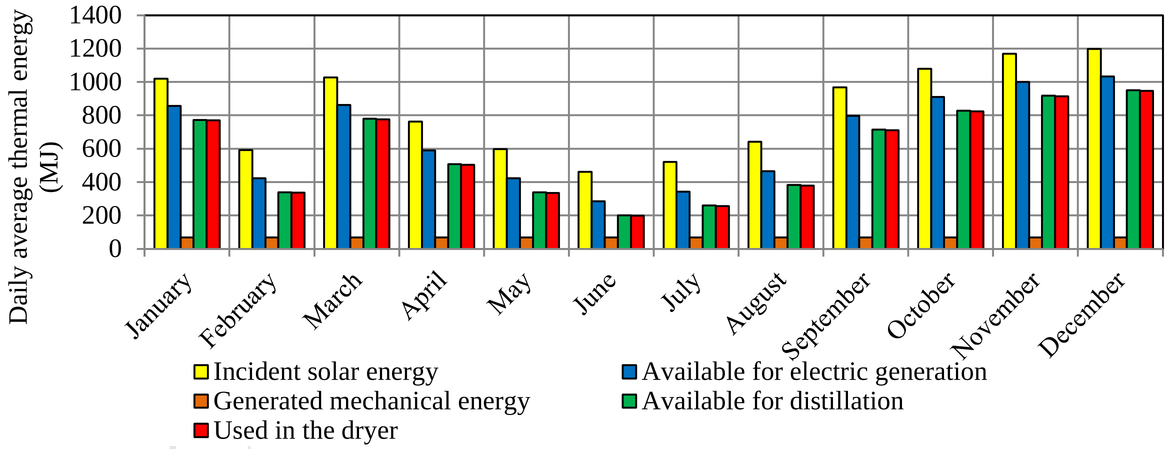

Figure 12. Incident solar thermal energy, energy available for desalination, energy available for power generation and energy used in the dryer, when steam is used to generate electrical energy.

The temperature of the steam decreases throughout the installation at a rate of -3.04 °C/m in summer and -3.13 °C/m in winter (Figure 13).

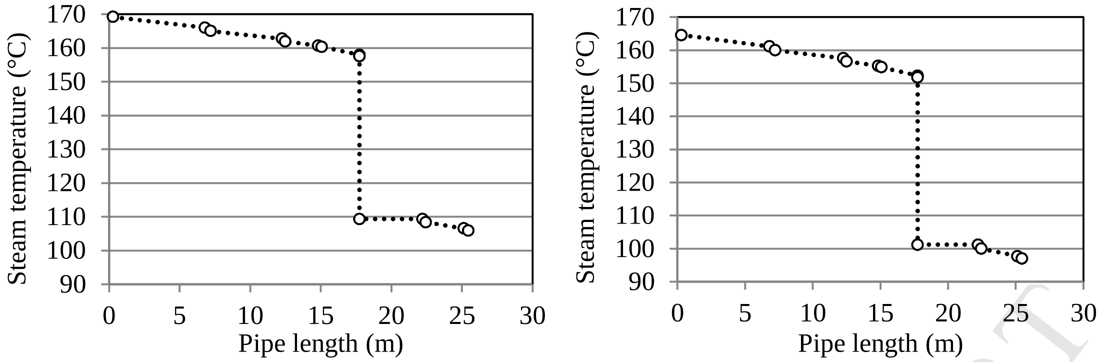

Figure 13. Temperature of steam through the pipe. Left: January. Right: June.

The thermal losses from engine head, together with the expansion work, produce a 40-50 °C decrease in the steam temperature. This thermal decrease is common in this type of low power thermal machines. It is observed that the temperature of the exhaust steam is around 100 °C, containing enough energy to be applied to desalination and drying processes.

5.3. Desalination of hard water

The amount of distillate depends on the technology that is used as well as the available thermal energy of the steam. In this case, a multi-stage distiller is connected to the main steam line, between the power block and the condenser, and its gain output ratio (GOR) is equal to 2.7 (Diaz 2017; Franco and Saravia, 1994). Equation 19 gives the amount of distillate in kg.

$$m_w = \frac{k \cdot E_a}{2.3\frac{MJ}{kg}} \cdot GOR \quad (19)$$

E_a is the thermal energy from the steam source, which can be complemented by direct solar gain (evacuated tubes) or electric resistances, if necessary. It is important to consider that not all of the thermal energy can be used in the desalination process, because the residual steam has to contain enough energy for the drying process. Therefore, the steam flow has to be regulated so that not all the thermal energy will be transferred to the water of the tank. This fact is considered by the k-factor in equation 19, which is assumed as k=0.4. Desalinated water production is summarized in Figure 14 with average daily values (it means, for characteristic days), when no mechanical energy (or electric power) is generated.

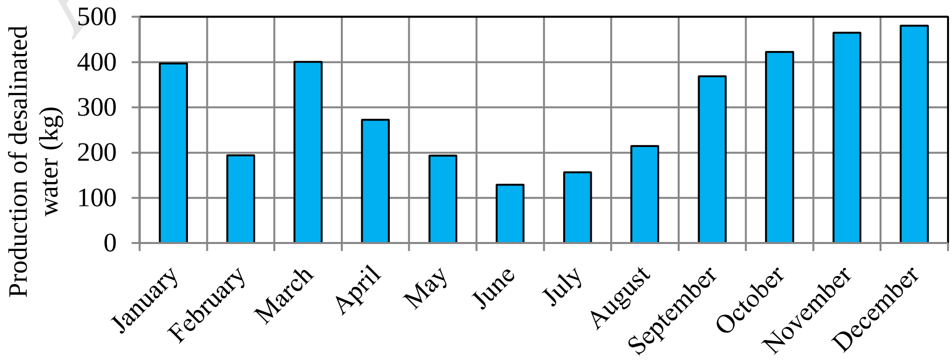

327 *Figure 14. Production of desalinated water; monthly average per day.*

328 Figure 15 shows the thermal energy involved in the processes. Production of desalinated
329 water causes an important decrease in the thermal energy available for the drying
330 process.

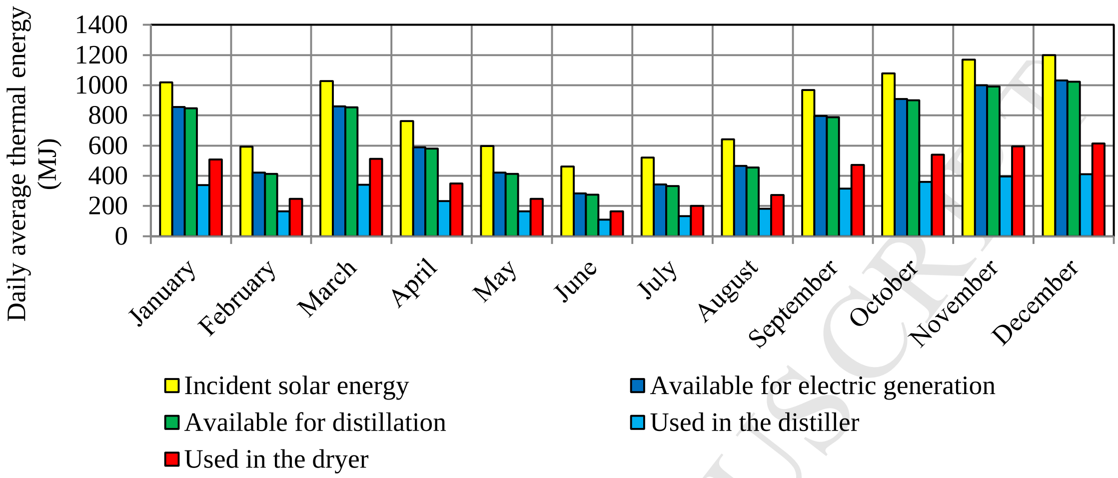

331
332 *Figure 15. Incident solar thermal energy, energy available for desalination, energy*
333 *available for power generation and energy used in the dryer, when steam is used for a*
334 *desalination process.*

335 *5.4. Desalination of hard water and electric power generation*

336 The steam is used for both processes, desalination of hard water and electric power
337 generation. Firstly, electric power is generated and the residual steam of this process is
338 used in the distiller. The power block generates the same amount of electric energy, but
339 the production of desalinated water decreases as shown in Figure 16.

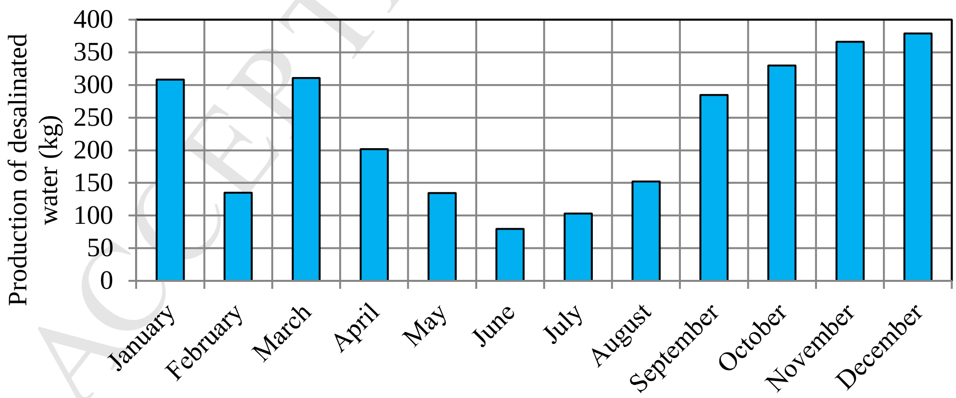

340
341 *Figure 16. Production of desalinated water; monthly average per day while electric*
342 *energy is generated.*

343 Now, the available thermal energy for the drying process is lower than that for the other
344 processes (Figure 17).

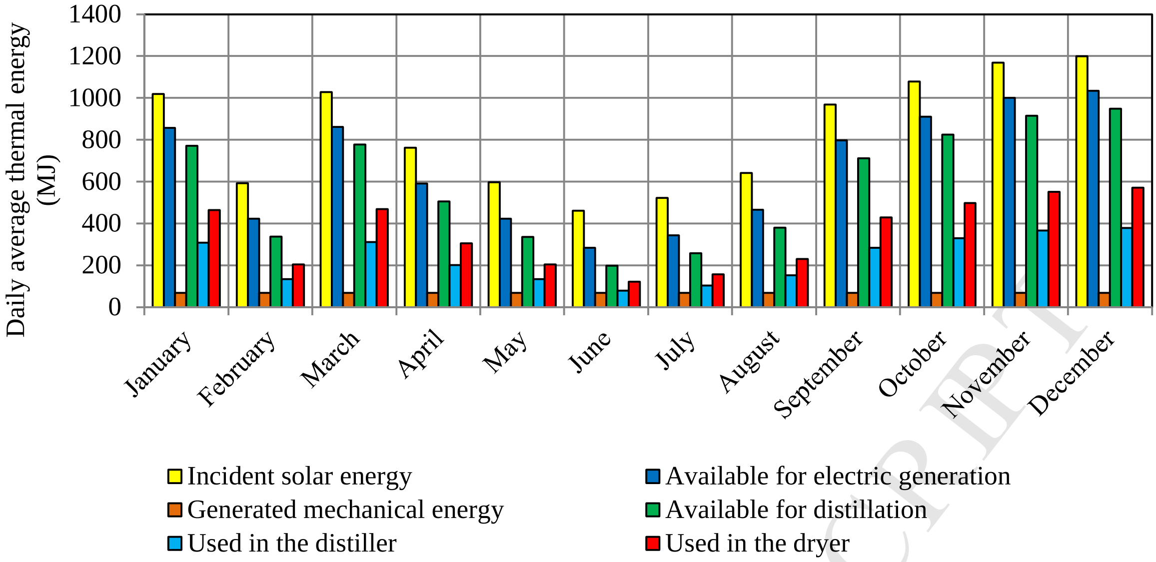

Figure 17. Incident solar thermal energy, energy available for desalination, energy available for power generation and energy used in the dryer, when steam is used for electric power generation and water desalination.

6. CONCLUSIONS

The present study performed the energy analysis of the LFS concentration system mounted in the city of San Carlos, Salta province, Argentina. The study was performed for the characteristic days of each month, with a covered absorber, and an operating time from 10 a.m. to 5 p.m. was assumed. The calculation of the energy absorbed by the HTF considers the measured values of the solar irradiation which reaches the mirror field, as well as the temperature of the steam generated by the equipment at the absorber outlet and working pressure.

Four scenarios for utilization of the steam were considered: direct steam injection into the condenser, electric power generation, desalinated water production and, finally, power generation and desalination together.

It was determined that the LFS generates steam with a daily average thermal energy of around 460-1200 MJ at the absorber outlet, according to the month and the solar irradiation available. It means 243 GJ accumulated per year. The availability of thermal energy for desalination processes ranges between 198 MJ (in winter, with electric power generation) and 10 GJ (in summer, without electric power generation). Lower values are obtained during the months of low solar irradiation. As a result, it would be convenient to take these values into account when implementing other desalination technology, since low values of thermal energy would demand the use of auxiliary systems to supply this energy lost in desalination processes. The multistage distiller proposed here is able to produce from 98 to 112 m^3 of pure water per year. Practically the same amount of energy at the absorber outlet is available for electric generation. A valve for steam deviation is mounted for this process before the desalination process, so the thermal energy available for desalination is lower because it uses exhaust steam from the steam engine. The power block can supply 5.2 GJ (1.5 GWh) annually, for a 288 rpm regime and working pressure of 6 bar. However, the electric supply varies with the electric load or consumption, and it affects the working pressure, temperature, thermal energy of the steam, and residual energy for the following process.

The steam temperature analysis reveals that it is necessary to improve the insulation of the pipes, particularly in sections where the valves are located. It is also observed that the thermal energy contained in the steam could be used for greater power generation, but for this goal a steam engine with higher performance is necessary. A more accurate estimate of the energy use could be obtained by more and better measurements in the different pieces of equipment. This involves the use of transducers and data loggers to measure pressures and temperatures instantaneously in each process, as well as the use of a central computer for the real-time recording of those parameters. As future work, the authors - and the work team of the Fresnel system of San Carlos - are developing a system for measuring and recording of temperatures, pressures and steam flow, with the aim of controlling such parameters by acting directly on the valves and the regulation of feed water flow.

Funding: This work was funded by MINCYT (Science and Technology Ministry of Argentina) through the PFIP 2009 project and by the Research Council of the National University of Salta through the project 2019/1.

7. REFERENCES

Alias D., Saravia L., Saravia D. Simusol: simulating thermal systems using SCEPTRE and DIA. J. Free Software Free Know, 1 (2012), pp. 30–34.

Altamirano M. (2014). Estudio de absorbedores para la generación de energía eléctrica mediante un reflector lineal tipo Fresnel. PhD thesis. National University of Salta. Argentina.

Ångström, A. (1961). Techniques of determining the turbidity of the atmosphere. Tellus 13, 214-223.

Baniasad Askari I. and Ameri M. Solar Rankine cycle (SRC) powered by linear Fresnel solar field and integratedwith multi effect desalination (MED) system. Renewable Energy. Volume 117, March 2018, Pages 52-70.

Barbón A, Barbón N, Bayón L, Sánchez-Rodríguez JA. Parametric study of the small scale linear Fresnel reflector. Renew Energy 2018;116:64–74.

Bermejo P, Pino FJ, Rosa F. Solar absorption cooling plant in Seville. Sol Energy 2010;84(8):1503–12.

Cagnoli M, Mazzei D, Procopio M, Russo V, Savoldi L, Zanino R. Analysis of the performance of linear Fresnel collectors: Encapsulated vs. evacuated tubes. Sol Energy 2018;164:119–38.

Carvalho M. J., Horta P., Farinha Mendes J, Collares Pereira M. and Maldonado Carbajal W. Incidence angle modifiers: a general approach for energy. 2007. Proceedings of ISES Solar World Congress 2007: Solar Energy and Human Settlement.

Condorí M., Durán G., Vargas D., Echazú R. (2009). Secador solar hibrido. Primeros ensayos. Avances en Energías Renovables y Medio Ambiente. Vol. 13.pps. 02.35 – 02.42. ISSN 0329-5184.

Cruz N.C., Redondo J.L., Berenguel M., Álvarez J.D. and P.M. Ortigosa. Review of software for optical analyzing and optimizing heliostat fields. Renewable and Sustainable Energy Reviews 72 (2017) 1001–1018.

Dellicompagni P., Franco J., Altamirano M., Hongn M. (2015). Caracterización de un motor a vapor de doble efecto. Avances en Energías Renovables y Medio Ambiente (AVERMA). Vol. 19.pp.03.01-03.12. ISSN 2314-1433.

Dellicompagni P., Hongn M., Saravia L., Altamirano M., Placco C., Gea M., Hoyos D., Bárcena H., Suligoy H., Fernández C., Caso R. (2016). Concentrador solar térmico Fresnel lineal de San Carlos. Salta. Primeros ensayos de operación y funcionamiento (172 m^2). Avances en Energías Renovables y Medio Ambiente Vol. 20, pp 03.01-03.12. ISSN 2314 – 1433.

Dellicompagni P., Saravia L., Altamirano M., Franco J. Simulation and testing of a solar reciprocating steam engine. Energy 151 (2018) 662 – 674.

Desai N., Kedare S., Bandyopadhyay S. Optimization of design radiation for concentrating solar thermal power plants without storage. Solar Energy 107 (2014) 98–112.

Díaz A. (2017). Análisis del funcionamiento de un destilador multi etapa con acumulador de calor por cambio de fase. Tesis de grado. Universidad Nacional de Salta, Argentina.

El Gharbi N., Derbal H., Bouaichaoui S., Said N. A comparative study between parabolic trough collector and linear Fresnel reflector technologies. Energy Procedia 6 (2011) 565 – 572.

Elsafi AM. On thermohydraulic modeling of direct steam generation. Sol Energy 2015;120:636–50.

Facão J., Oliveira A. Numerical simulation of a trapezoidal cavity receiver fora linear Fresnel solar collector concentrator. Renewable Energy 36 (2011) 90 – 96.

Feuermann D., Gordon J. M. Analysis of a two-stage linear Fresnel reflector solar concentrator. Journal of Solar Energy Engineering, Transactions of the ASME November 1991; 113:272 – 9.

Flores Larsen S., Altamirano M., Hernández A. Heat loss of a trapezoidal cavity absorber for a linear Fresnel reflecting solar concentrator. Renewable Energy 39 (2012) 198 – 206.

Flores Larsen S., Hongn M. Determining the infrared reflectance of specular surfaces by using thermo-graphic analysis. Renewable Energy 64 (2014) 303 – 313.

Franco J., Saravia L. A new design for a passive atmospheric multi stage still. Renewable Energy, Vol. 4, No. I, pp. 119 122. 1994.

Goswami Y., Kreith F. 2008. Energy Conversion. CRC Press. FL.

Grossi Gallegos H. y Righini R. (2007). Atlas de Energía Solar de la República Argentina. Universidad Nacional de Luján. Secretaría de Ciencia y Tecnología. Buenos Aires. Argentina. ISBN 978-987-9285-36-7.

Grossi Gallegos H., Aristegui R., Righini R. (2009). Análisis de la radiación solar global en San Carlos, Salta. Avances en Energías Renovables y Medio Ambiente Vol. 13. ISSN 0329-5184.

Häberle A., Zahler C., Lerchenmüller H., Mertins M., Wittwer C., Trieb F. The Solarmundo line focussing Fresnel collector. Optical and thermal performance and cost calculations. Zürich. International symposium on concentrated solar power and chemical energy technologies. 2002.

Hachicha AA, Rodríguez I, Ghenai C. Thermo-hydraulic analysis and numerical simulation of a parabolic trough solar collector for direct steam generation. Appl. Energy 2018;214:152–65.

Heimsath A, Nitz P, Heß S. Concentrating solar collectors for process heat up to 250 °C and small scale CSP – Integrated optical design for improved performance. EuroSun2010; 2010.

Hongn M. (2017). Estudio y evaluación de parámetros de funcionamiento para la tecnología Fresnel lineal de concentración. PhD thesis. National University of Salta. Argentina.

Hongn M., Flores Larsen S. Hydrothermal model for small-scale linear Fresnel absorbers with non-uniform stepwise solar distribution. Applied Energy 223 (2018) 329 – 346.

Hongn M., Flores Larsen S., Dellicompagni P., Hoyos D., Fernández C., Suligoy H., Bárcena H., Gea M., Saravia L. (2015). Simulación del comportamiento hidrotérmico del fluido de trabajo en un concentrador Fresnel lineal. Energía Renovable y Medio Ambiente. Vol. 36. pp. 1 - 10. 2015. ISSN 0328-932X.

John A. Duffie & William A. Beckman. (2005). Solar Engineering of Thermal Processes. Third Edition. John Wiley and Sons.

Khan Md KA. Technical note: Copper oxide coating for use in a linear solar Fresnel reflecting concentrating collector. Renewable Energy 17 (1999) 603 – 608.

Lin M., Sumathy K., Dai Y. J., Wang R.Z., Chen Y. Experimental and theoretical analysis on a linear Fresnel reflector solar collector prototype with V-shaped cavity receiver. Applied Thermal Engineering 51 (2013) 963 – 972.

Mertins, M., 2008. Technische und wirtschaftliche Analyse von horizontalen Fresnel-Kollektoren, PhD thesis. http://digbib.ubka.uni-karlsruhe. de/volltexte/1000013884.

Mittelman G., M. Epstein. A novel power block for CSP systems. Solar Energy 84 (2010) 1761–1771.

Mokhtar G, Boussad B, Noureddine S. A linear Fresnel reflector as a solar system for heating water: theoretical and experimental study. Case Stud Therm Eng 2016;8:176–86.

Morin G, Dersch J, Platzer W, Eck M, Haberle A. Comparison of linear Fresnel and parabolic trough collector power plants. Sol Energy 86 (2012) 1 – 12.

Murphy L. M., Kennet May E. Steam Generation in line-Focus Solar Collectors: A Comparative Assessment of Thermal Performance, Operating Stability and Cost Issues. (1982). Solar Energy Research Institute. U.S. Department of Energy.

Negi B. S., Mathur S. S., Kandpal T. C. Optical and thermal performance evaluation of a linear Fresnel reflector solar concentrator. Solar & Wind Technology. Volume 6, Issue 5, 1989, Pages 589 – 593.

Patel. M. R.Wind and solar power systems: design, analysis and operation. 2nd ed. Florida (USA): CRC Press; 1999. ISBN0849315700.

Qui Yu, Li Ming-Jia, Wang Kun, Liu Zhan-Bin, Xue Xiao-Dai. Aiming strategy optimization for uniform flux distribution in the receiver of a linear Fresnel solar reflector using a multi-objetive genetic algorithm. Appl Energy 2017;205:1394–407.

Raichijk C. Grossi Gallegos H. Righini R. (2008). Cartas preliminares de irradiación directa para Argentina. Avances en Energías Renovables y Medio Ambiente. Vol. 12. pp. 11.01 -11.07 versión CD-ROM.

Rawlins J, Ashcroft M. Report: small scale concentrated solar power – a review of current activity and potential to accelerate employment, carbon trust; 2013. Available at:<https://www.gov.uk/government/uploads/system/uploads/attachment_data/file/191058/small_scale_concentrated_solar_power_carbon_trust.pdf>.

Saravia L., Gea M., Hongn M., Hoyos D., Barcena H., Placco C., Cadena C., Flores Larsen S., Dellicompagni P., Condorí M., Martínez C., Fernández C., Caso R., Altamirano M., Suligoy H. (2014). Descripción de un generador solar térmico de tipo

Fresnel instalado en San Carlos. Salta. Avances en Energías Renovables y Medio Ambiente. Vol. 18. pp. 03.17 – 03.26. ISSN 2314 – 1433.

Serrano-Aguilera JJ, Valenzuela L, Parras L. Thermal hydraulic RELAP5 model for a solar direct steam generation system based on parabolic trough collectors operating in once-through mode. Energy 2017;133:796–807.

Singh P. L., Sarviya R. M., Bhagoria J. L. Heat loss study of trapezoidal cavity absorbers for linear solar concentrating collector. Energy Conversion and Management 57 (2010) 329 – 337.

Singh P. L., Sarviya R. M., Bhagoria J. L. Thermal performance of linear Fresnel reflecting solar concentrator with trapezoidal cavity absorbers. Applied Energy 87 (2010) 541–550.

Sistema de Información Geográfica Eólico del Centro Regional de Energía Eólica. http://sigeolico.minplan.gob.ar/pmapper_demo/frameview.phtml?language=0.

Sultana T, Morrison GL, Rosengarten G. Thermal performance of a novel rooftop solar micro-concentrating collector. Sol Energy 2010;86(7):1992–2000.

Theodore L. Bergman, Adrienne S. Lavine, Frank P. Incropera, David P. Dewitt.. Fundamentals of Heat and Mass Transfer. Seventh edition. John Wiley and Sons. ISBN 13 978 – 0470 – 50197 – 9.

Tsekouras P, Tzivanidis C, Antonopoulos K. Optical and thermal investigation of a linear Fresnel collector with trapezoidal cavity receiver. Appl Therm Eng 2018;135:379–88.

Velázquez N, García-Valladares O, Sauceda D, Beltrán R. Numerical simulation of a linear Fresnel reflector concentrator used as direct generator in a solar-GAX cycle. Energy Convers Manage 2010;51:434–45.

W.H. Mc Adams. Heat Transmission. 3rd Edition (New York, New York: McGraw-Hill Book Co., 1954).

Wagner M. and Zhu G.A direct-steam linear Fresnel performance model for NREL's System Advisor Model (SAM). 2012. Proceedings of the ASME 2012 6th International Conference on Energy Sustainability and 10th Fuel Cell Science, Engineering and Technology Conference.

Yang K., G. W. Huang y Tamai N. (2001). A hybrid model for estimating global solar radiation. Solar Energy 70, 1, 13 – 22.

Zhou L, Li X, Zhao Y, Dai Y. Performance assessment of a single/double hybrid effect absorption cooling system driven by linear Fresnel solar collectors with latent thermal storage. Sol Energy 2017;151:82–94.

Zhu J, Chen Z. Optical design of compact linear Fresnel reflector systems. Sol Energy Mater Sol Cells 2018;176:239–50.

Highlights

- The energy analysis of the LFS concentration system mounted in the city of San Carlos, Salta province, Argentina was performed.
- Thermal losses at the absorber cavity as well as field pipes were determined.
- Available thermal energy for different applications was determined.
- It was determined that the LFS generates steam with a daily average thermal energy of around 460-1200 MJ at the absorber outlet.

Nomenclature

A_{abs}	Absorber external area (m^2)
A_i	Area of each mirror (m^2)
d_i	Inner diameter of field pipe (m)
D_i	Inner diameter of PVC® cover (m)
DNI	Direct normal irradiance (W/m^2)
d_o	Outer diameter of field pipe (m)
D_o	Outer diameter of field PVC® cover (m)
E_a	Thermal energy from the steam source (MJ)
EE	Electric power (kWh_e)
F	Brake force (lb_f)
F_e	Cleanliness factor (dimensionless)
f_i	Illuminated fraction of the absorber (dimensionless)
F_i	Intercept factor of receiver (dimensionless)
f_{l0}	Steam flux (kg/s)
GOR	Gain output ratio (dimensionless)
h_a	Convection coefficient of the external air (W/m^2K)
h_{conv}	Convective coefficient of steam inside the pipe (W/m^2K)
h_0	Steam specific enthalpy at section 0 for control volume (J/kg)
h_1	Steam specific enthalpy at section 1 for control volume (J/kg)
h_r	Linear coefficient of radiation to the environment (W/m^2K)
k	Portion of E_a used for desalination (dimensionless)
k_{ais}	Conductive coefficient of isolation (W/mK)
k_{PVC}	Conductive coefficient of PVC® cover (W/mK)
k_w	Conductive coefficient of pipe wall (W/mK)
L	Field pipe length (m)
m_w	Amount of distillate (kg/day)
n	Speed regime of steam engine (rpm)
N_u	Effective mechanical power developed by the steam engine (W)
$\dot{Q}_a$	Average hourly thermal power (W)
$\dot{Q}i$	Incident thermal power (W)
$\dot{Q}_j$	Total heat loss at each point of the installation (W)
$\dot{Q}_l$	Heat loss to environment through field pipes (W)
T_e	Environmental temperature (K)
T_f	Steam temperature (K)
T_o	Temperature of external surface of the non-insulated section (K)
T_{pipe}	External temperature of pipes (K)
U_L	Heat loss coefficient (W/Km^2)
x_0	Steam fraction at section 0 for control volume (dimensionless)
x_1	Steam fraction at section 1 for control volume (dimensionless)

Greek symbols

α	Absorptivity of pipes surface (dimensionless)
$\delta\theta$	Variation in steam temperature (K)
δx	Variation in steam fraction (dimensionless)
$\Delta\dot{Q}_{ia}$	Thermal losses from the absorber to environment (W)
$\Delta\dot{Q}_{l-i}$	Thermal losses toward environment by insulated pipes (W)
$\Delta\dot{Q}_{l-n}$	Thermal losses toward environment by non-insulated pipes (W)
ε	Emissivity of external surface of the non-insulated pipes (dimensionless)
η_{gr}	Efficiency of electric generator (dimensionless)
η_{th}	Thermal efficiency of the absorber (dimensionless)
η_{tr}	Efficiency of mechanical transmission of power block (dimensionless)
θ_0	Steam temperature at section 0 for control volume (K)
θ_1	Steam temperature at section 1 for control volume (K)
θ_i	Incidence angle (º)
ρ_1	Steam density at section 1 for control volume (kg/m^3)
ρ_g	Gas phase density (kg/m^3)
ρ_i	Reflectance of each mirror (dimensionless)
ρ_l	Liquid phase density (kg/m^3)
σ	Stefan-Boltzmann constant (5.670373×10^{-8} W/s^{3}K^4)
τ	Transmittance of glass cover (dimensionless)